Research Article

Bhargav Akkinepally[#], Bairi Sri Harisha[#], Nandini Robin Nadar, Muhammad Altaf Nazir, Ammar M. Tighezza, Himadri Tanaya Das, Itheereddi Neelakanta Reddy, Jaesool Shim*, and Dongwhi Choi*

Nanoscale synergy: Optimizing energy storage with SnO₂ quantum dots on ZnO hexagonal prisms for advanced supercapacitors

https://doi.org/10.1515/ntrev-2024-0047 received March 27, 2024; accepted June 3, 2024

Abstract: Electrode materials comprising SnO₂ quantum dots embedded within ZnO hexagonal prisms were successfully synthesized for building cost-effective energy-storage devices. Extensive structural and functional characterizations were performed to assess the electrochemical performance of the electrodes. SEM–EDS results confirm a uniform distribution of SnO₂ quantum dots across ZnO. The integration of SnO₂ quantum dots with ZnO hexagonal prisms markedly improved the electrochemical behavior. The analysis of electrode functionality conducted in a 3 M KOH electrolyte revealed specific capacitances of 949.26 and 700.68 F g⁻¹ for SnO₂@ZnO and ZnO

These authors contributed equally to this work and should be considered first co-authors.

Bhargav Akkinepally: School of Mechanical Engineering, Yeungnam University, Gyeongsan, 38541, Republic of Korea; School of General Education, Yeungnam University, Gyeongsan, 38541, Republic of Korea Bairi Sri Harisha, Itheereddi Neelakanta Reddy: School of Mechanical Engineering, Yeungnam University, Gyeongsan, 38541, Republic of Korea Nandini Robin Nadar: International Institute of Aerospace Engineering & Management (IIAEM), Jain University-Global Campus, 562112, Bangalore, India

Muhammad Altaf Nazir: Institute of Chemistry, The Islamia University of Bahawalpur, Bahawalpur 63100, Pakistan

Ammar M. Tighezza: Department of Chemistry, P. O. Box 2455, College of Science, King Saud University, Riyadh 11451, Saudi Arabia

Himadri Tanaya Das: Department of Physics, Utkal University, Vanivihar, 751004, Bhubaneswar, India

electrodes, respectively, under a current density of 2 A g⁻¹. After undergoing 5,000 cycles at a current density of 15 A g⁻¹, the SnO₂@ZnO and ZnO electrodes displayed impressive cycling stability, maintaining specific capacitance retention rates of 89.9 and 92.2%, respectively. Additionally, a symmetric supercapacitor (SSC) device constructed using the SnO2@ZnO electrode showcased exceptional performance, exhibiting a specific capacitance of 83 F g⁻¹ at 1.2 A g⁻¹. Impressive power and energy densities were achieved by the device, with values reaching 2,808 and 70.2 W kg⁻¹, respectively. Notably, the SnO₂@ZnO SSC device maintained a capacity preservation of 75% throughout 5,000 galvanostatic charge-discharge sequences. The outcomes highlight the potential of SnO₂@ZnO hexagonal prisms as candidates for energy-storage applications, offering scalability and cost-effectiveness. The proposed approach enhances the electrochemical performance while ensuring affordability, facilitating the creation of effective and financially feasible energy storage solutions.

Keywords: supercapacitors, energy storage, SnO₂ quantum dots, ZnO hexagonal prisms, symmetric supercapacitor

1 Introduction

The increasing need for clean and sustainable energy solutions has accelerated the advancement of effective energy storage devices [1–6]. Supercapacitors, also known as electrochemical capacitors, have emerged as potential candidates because of their unique characteristics [7]. They serve as a link between traditional capacitors and batteries, offering superior power density than batteries and remarkable energy density than capacitors [8,9]. This translates to exceptionally fast charge/discharge cycles, making them ideal for applications that require instantaneous power delivery and uptake (such as in electric vehicles), integration of renewable energy sources into the grid, and portable

^{*} Corresponding author: Jaesool Shim, School of Mechanical Engineering, Yeungnam University, Gyeongsan, 38541, Republic of Korea, e-mail: jshim@ynu.ac.kr

^{*} Corresponding author: Dongwhi Choi, Department of Mechanical Engineering (Integrated Engineering Program), Kyung Hee University, 1732 Deogyeong-daero, Yongin, Gyeonggi, 17104, Republic of Korea, e-mail: dongwhi.choi@khu.ac.kr

electronics [10]. Despite their immense potential, supercapacitors still face challenges that limit their widespread application, particularly in the identification and development of effective electrode materials [11,12]. Ideally, these materials should possess a synergistic combination of properties, such as high capacitance, excellent rate capability, and extended cyclic stability [13]. A high capacitance corresponds to the capacity to store a significant quantity of electrical energy, directly affecting the energy density of a supercapacitor device [14,15]. To achieve excellent rate capability, the electrode material should allow for rapid charge/discharge cycles, ensuring that the supercapacitor can deliver and absorb energy quickly [16]. This attribute is vital for scenarios necessitating frequent bursts of power, such as the acceleration of electric vehicles. In addition to achieving extended cycling stability, the developed supercapacitors should undergo degradation, resulting in a gradual decline in capacitance over time. Electrodes with exceptional cycling stability can maintain their performance for long durations, thereby extending the lifespan of the device [17]. In this regard, metal oxides [18] have been extensively explored for supercapacitor electrodes (cerium dioxide [19], iron(III) oxide [20]) because of their abundance, environmental friendliness, and inherent electrochemical properties. SnO₂ and ZnO are two prominent materials in this category [21–23]. ZnO is acknowledged as a versatile semiconductor with notable electrical conductivity, reaching up to 230 S/cm [24,25]. The ability to adjust the bandgap, morphology, and size of ZnO allows for its extensive utilization across various device technologies [26]. ZnO offers several advantages, including a high theoretical capacitance, good environmental stability, and relatively high conductivity compared to that of other metal oxides [27]. However, ZnO suffers from fast capacitance decay during charge/discharge cycles. This rapid degradation significantly reduces the long-term performance and stability of a supercapacitor [28]. SnO₂ boasts several attractive features for supercapacitor applications. It possesses a high theoretical capacitance, indicating its potential to store significant amounts of electrical energy [29,30]. Additionally, SnO₂ exhibits pseudocapacitive behavior, a mechanism that enhances the capacitance compared with the pure electrical double-layer capacitance [31]. However, a significant drawback of using SnO2 is its low electrical conductivity, which hinders the efficient transfer of electrons within the electrode, ultimately affecting the rate capability of the supercapacitor [32]. Hence, research endeavors have concentrated on mitigating the drawbacks of individual metal oxides and exploring composite materials that leverage the strength of each component [33]. In this context, the utilization of SnO₂-decorated ZnO hexagonal prisms shows promise in advancing the development of high-performance supercapacitor electrodes. However,

working on SnO₂/ZnO composites for supercapacitor applications may reveal a gap in knowledge regarding the specific design and morphology of the composite material for optimal performance. The use of ZnO hexagonal prisms as a scaffold decorated with SnO2 nanoparticles offers a unique approach with several potential benefits. The hexagonal prismatic structure of ZnO provides a large surface area to accommodate the deposition of SnO₂ nanoparticles [34]. This increased surface area can enhance the number of electrochemically active sites available for charge storage, potentially leading to higher capacitance. Further decoration of the ZnO hexagonal prisms with well-dispersed SnO₂ quantum dots can improve the overall conductivity of the composite electrode. This addresses the limitations of pristine SnO₂ while retaining its high theoretical capacitance. Thus, the combination of SnO₂ and ZnO could potentially generate a synergistic effect in which the advantages of each material complement the other. For instance, SnO₂ can enhance the capacitance of a composite, whereas ZnO can improve its cycling stability.

This study aims to bridge this knowledge gap by comprehensively investigating SnO₂-decorated ZnO hexagonal prisms as supercapacitor electrodes. We explored the synthesis of these composite materials with controlled morphology and tailored SnO₂ loading. Extensive testing was conducted to evaluate the electrochemical performance of the electrodes, with specific attention given to capacitance, rate capability, and cycling stability. A detailed analysis was conducted to decipher the structure–property relationships between the morphology, composition, and resulting electrochemical behavior of the composite electrodes by unveiling the performance potential and underlying mechanisms of SnO₂-decorated ZnO hexagonal prisms.

2 Materials and methods

2.1 Material synthesis and preparation

2.1.1 SnO₂ quantum dots

To prepare SnO_2 quantum dots, 2.5 g of $SnCl_4$ - SH_2O (Daejung Chemicals and Metals Co., Korea) was dissolved in DI water (130 ml) and agitated at 600 rpm for 5 min. Subsequently, 5.3 ml of hydrazine (N_2H_4 – Sigma-Aldrich, USA) was gradually added dropwise to the solution while maintaining the agitation for 20 more minutes at a temperature of 25°C. The solution was then heated to 105°C (in the absence of agitation) for 19 h. The residue from the mixture was retrieved via centrifugation, followed by thorough washing with water and ethanol, typically lasting 4–5 cycles. Following that, it was placed in an oven at 75°C and dried for 14 h.

2.1.2 SnO₂ quantum dots interspersed ZnO hexagonal prisms

To prepare SnO₂-decorated ZnO nanostructures, equivalent amounts of commercially obtained ZnO (Sigma-Aldrich, USA) and synthesized SnO₂ quantum dots were separately dispersed in 50 ml of water and stirred for 60 min to achieve a homogeneous liquid solution. Subsequently, the SnO₂based solution was added dropwise to the ZnO solution under continuous stirring for 3h at room temperature (25°C). Following that, the resulting material was subjected to centrifugation and washed with water and ethanol four to six times, followed by drying for 20 h at 80°C in a hot air oven.

2.2 Electrode fabrication

The assembly process of the working electrode entailed the meticulous application of a slurry onto a Ni-foam using the drop-casting technique. Ethanol was added to ensure a homogeneous mixture, which was then uniformly applied to pre-cleaned and pre-weighed Ni-foam substrates (1 × 1 cm²). The slurry was prepared by mixing the active material with carbon spheres, which served as an electrically conductive additive, in a weight ratio of 8:2. The active material was loaded onto each electrode at a mass of approximately 1 mg. Following that, the electrodes were dried overnight at 80°C to eliminate any residual solvent and ensure the formation of well-defined electrode structures.

2.3 Electrochemical performance assessment

In the electrochemical setup, an Ag/AgCl and a Pt wire were utilized as the reference electrode and counter electrode, respectively. An active material (ZnO, SnO₂, or SnO₂@ZnO) drop-cast onto a Ni-foam substrate served as the working electrode. All electrochemical assessments were carried out in a 3.0 M KOH electrolyte. Several analytical methods were used to explore the electrochemical attributes. Cyclic voltammetry (CV) was employed to examine the redox characteristics of the electrodes. To investigate the charge-transfer resistance and interfacial features, electrochemical impedance spectroscopy (EIS) was used. To assess the energy-storage capabilities of the electrodes, galvanostatic charge/ discharge (GCD) analyses were employed. A potentiostat instrument (SP-200 Bio-Logic) was utilized to assess all the electrochemical evaluations.

2.4 Device assembly and testing

To assemble the symmetric supercapacitor (SSC) device, SnO₂@ZnO was deposited onto Ni-foam, fulfilling the roles of both positive and negative electrodes. A 3.0 M KOH solution was used as an electrolyte. CV of the device was performed by employing incremental sweep rates from 5 to 200 mV s⁻¹ under a potential span of 0–1.3 V. GCD analysis was carried out by employing current densities ranging from 1.2 to 2 A g⁻¹. Furthermore, EIS assessments were conducted within a frequency range of 200 kHz to 0.1 Hz using an open circuit voltage. The specific capacitance (C_s) was calculated using the following equation:

$$C_{\rm S} = \frac{I \cdot \Delta t}{m \cdot \Lambda V},\tag{1}$$

where I stands for the applied current (A), Δt signifies the discharge time (s), ΔV indicates the voltage window (V), m represents the active material mass (g), and C_s denotes the specific capacitance (F g⁻¹). The following equations were used to calculate the energy density (E_d) and power density $(P_{\rm d})$ of the system:

$$E_{\rm d} = \frac{1}{2} C_{\rm s} (\Delta V)^2, \tag{2}$$

$$P_{\rm d} = \frac{E_{\rm d}}{\Lambda t}.$$
 (3)

3 Results and discussion

3.1 Material characterization

X-ray diffraction (XRD) was utilized to examine the crystalline properties of ZnO, SnO₂, and SnO₂@ZnO, and the obtained XRD data are presented in Figure 1. All the discernible peaks of ZnO are precisely indexed and aligned with JCPDS card No. 75-1526, confirming its high crystallinity. A prominent high-intensity peak is observed at 36.1°, corresponding to the (101) plane of hexagonal ZnO. The XRD pattern for the SnO₂ quantum dots exhibits peaks at 26.2° (110), 33.6° (101), and 51.8° (211), indicating a tetragonal crystal structure (JCPDS card No. 77-0450). The XRD peaks for the SnO2-decorated ZnO nanostructure include one at 36.5°, corresponding to the (101) plane, with a slight increase attributed to SnO2. Importantly, the hexagonal crystal structure of the ZnO nanostructure remains unaffected, indicating that the introduction of SnO₂ does not alter the ZnO structure but rather enhances its crystallinity. The X-ray intensity initially exhibits a maximum on the surface of SnO₂ compared to that in the ZnO

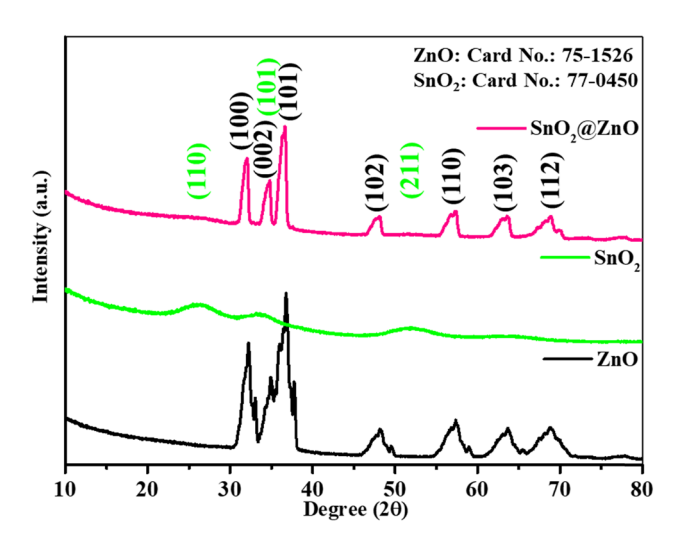


Figure 1: XRD patterns for ZnO hexagonal prisms (ZnO), SnO_2 quantum dots (SnO_2), and SnO_2 quantum dot-decorated ZnO hexagonal prisms ($SnO_2@ZnO$).

nanostructure because the characteristic peaks of ZnO have higher intensities in the SnO₂@ZnO samples. Information on the interplanar distance, particle size, and strain was obtained from the XRD results utilizing Bragg's law,

Scherrer's formula, and the Williamson–Hall formula, respectively. The interplanar distance d (101) increased in the $SnO_2@ZnO$ sample, indicating the introduction of smaller Sn atoms into the lattice. The crystalline sizes for (100), (101), (102), and (110) peaks were increased in $SnO_2@ZnO$ when compared to pristine ZnO but remained constant for the (002) peak. This can be due to the interaction between SnO_2 and ZnO that may alter the surface energy of the composite material, affecting the kinetics of crystal growth differently for various crystallographic planes. These subtle variations in size can be attributed to differences in the growth mechanisms, preparation temperatures, and particle sizes. The observed distinctions align with prior reports on similarly decorated compounds, confirming the successful decoration of SnO_2 on ZnO.

Examination of the morphology of the samples was carried out by utilizing field emission scanning electron microscopy (FESEM), as shown in Figure 2(a)–(c). The FESEM images reveal hexagonal prisms with an irregular size distribution for the ZnO nanocrystals. Figure 2(b) shows large grains of SnO₂ with irregular shapes, likely resulting from particle accumulation owing to the reaction conditions. Rapid nucleation facilitates the even distribution of

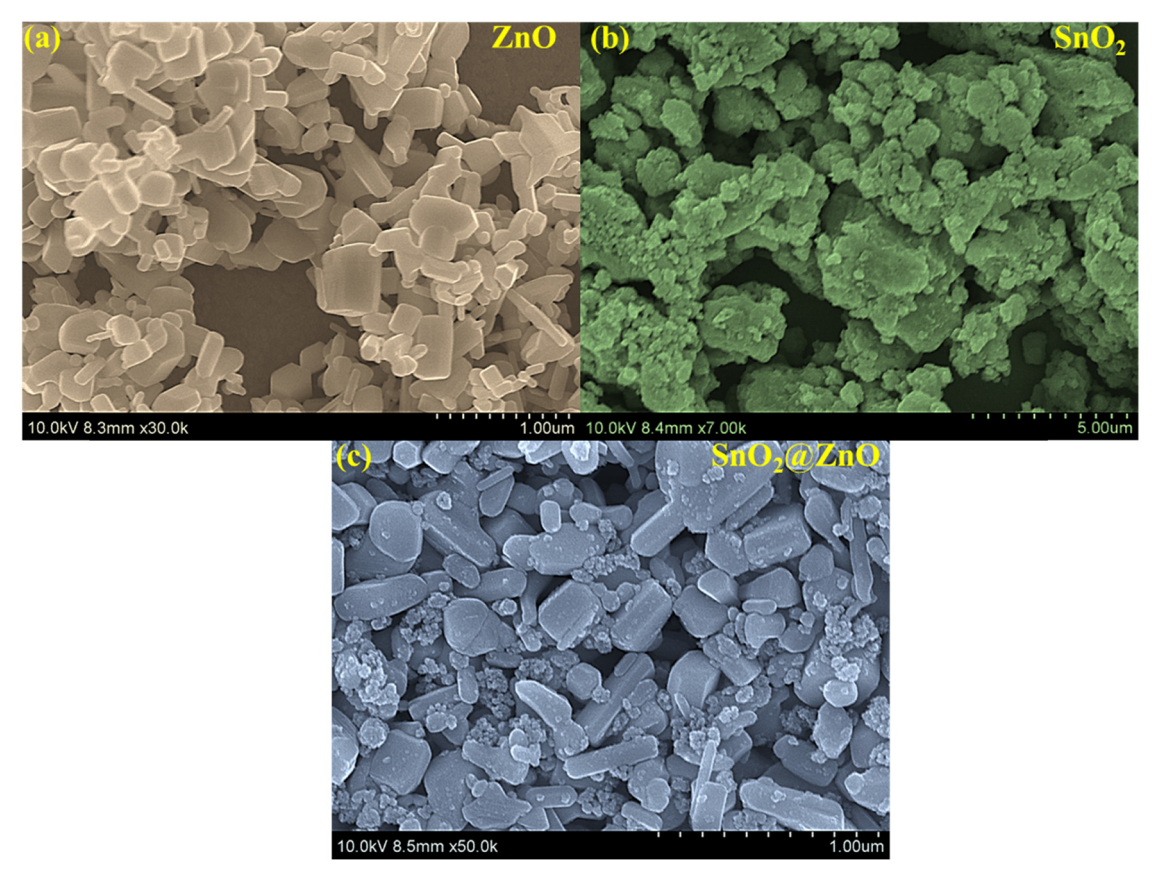


Figure 2: SEM analysis of (a) ZnO hexagonal prisms, (b) SnO₂ quantum dots, and (c) SnO₂@ZnO hexagonal prisms.

SnO₂ quantum dots over the ZnO hexagonal nanostructure, as observed in Figure 2(c).

The morphological characteristics of SnO₂@ZnO were further investigated by field emission transmission electron microscopy (FETEM). Figure 3(a)–(c) presents FETEM images of the SnO₂@ZnO hexagonal prisms. Upon magnification, the FETEM micrographs present well-defined lattice fringes, indicating interplanar spacings of 0.47 nm (ZnO) and 0.33 nm (SnO₂) (Figure 3(b) and (c)). The selected area electron diffraction (SAED) pattern (Figure 3(d)) conclusively illustrates the polycrystalline nature of the SnO₂@ZnO hexagonal prisms, revealing interconnected nanostructures [35]. The results align with the XRD findings, offering additional confirmation of the effective amalgamation of SnO2 quantum dots and ZnO nanostructures. Additionally, the elemental distribution within the SnO₂@ZnO specimen is shown in Figure 3(e)-(h) illustrates the EDS mapping. The homogeneous dispersion of core elements across the sample, revealed by the mapping, suggests a uniform distribution.

Porosity and specific surface area characteristics were also assessed through Brunauer–Emmett–Teller (BET) analysis (Figure 4). Nitrogen adsorption–desorption isotherms of the specimens display a distinct type IV hysteresis, featuring a loop at relative pressures between 0.9 and 1.0, which signifies the existence of mesopores, as depicted in Figure 4(a). This mesoporous configuration aids in minimizing the electron transport distance, thereby optimizing

the electron transfer efficiency [36]. In Figure 4(b), the average pore diameters are shown to be 3.6 nm for ZnO and 2.7 nm for SnO₂@ZnO, employing the Barrett–Joyner–Halenda (BJH) method. These results indicate the presence of a conventional mesoporous configuration in both samples [37]. The BET surface area measurements (Figure 4(c)) reveal values of 3.91 m²/g for ZnO and 9.39 m²/g for SnO₂@ZnO, demonstrating a threefold rise in surface area ascribed to the decoration of SnO₂ onto ZnO. This enhancement in surface area is evident in the comparative electrochemical performance analysis of the two electrodes.

X-ray photoelectron spectroscopy (XPS) is a suitable technique for examining the chemical structure of samples. In this study, ZnO hexagonal prisms, SnO2 quantum dots, and SnO₂@ZnO hexagonal prisms were subjected to XPS analysis, as shown in Figure 5(a). The core element peaks of Zn, Sn, and O are identified at their predicted positions, indicating high quality of the samples. The Zn 2p spectra for pure ZnO and SnO₂@ZnO (Figure 5(b) and (c)) reveal two strong peaks at energies of 1021.2 eV and 1044.3, corresponding to the Zn 2p_{3/2} and Zn 2p_{1/2} lines, respectively. The difference of 23.1 eV between these energy levels indicates the oxidation state of Zn to be +2 [38]. Similarly, the results in Figure 5(d) and (e) indicate that Sn is in the +4 oxidation state, confirmed by two strong peaks occurring at energies of 486.1 and 494.5 eV, equivalent to Sn 3d_{5/2} and Sn 3d_{3/2}, respectively. A distinction of 8.4 eV between the major Sn peaks corresponds to the energy variance. No significant

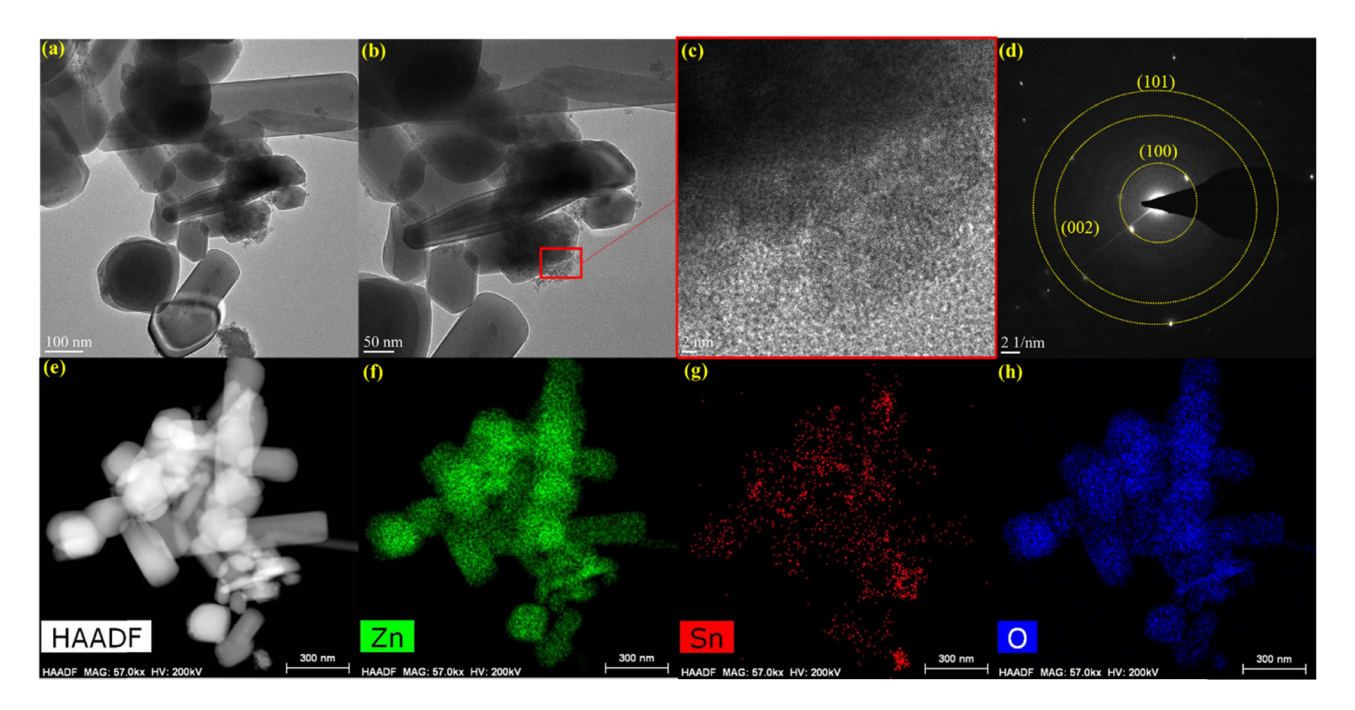


Figure 3: (a)–(c) FETEM images of SnO₂@ZnO, (d) SAED patterns of SnO₂@ZnO, and (e)–(h) EDS mapping.

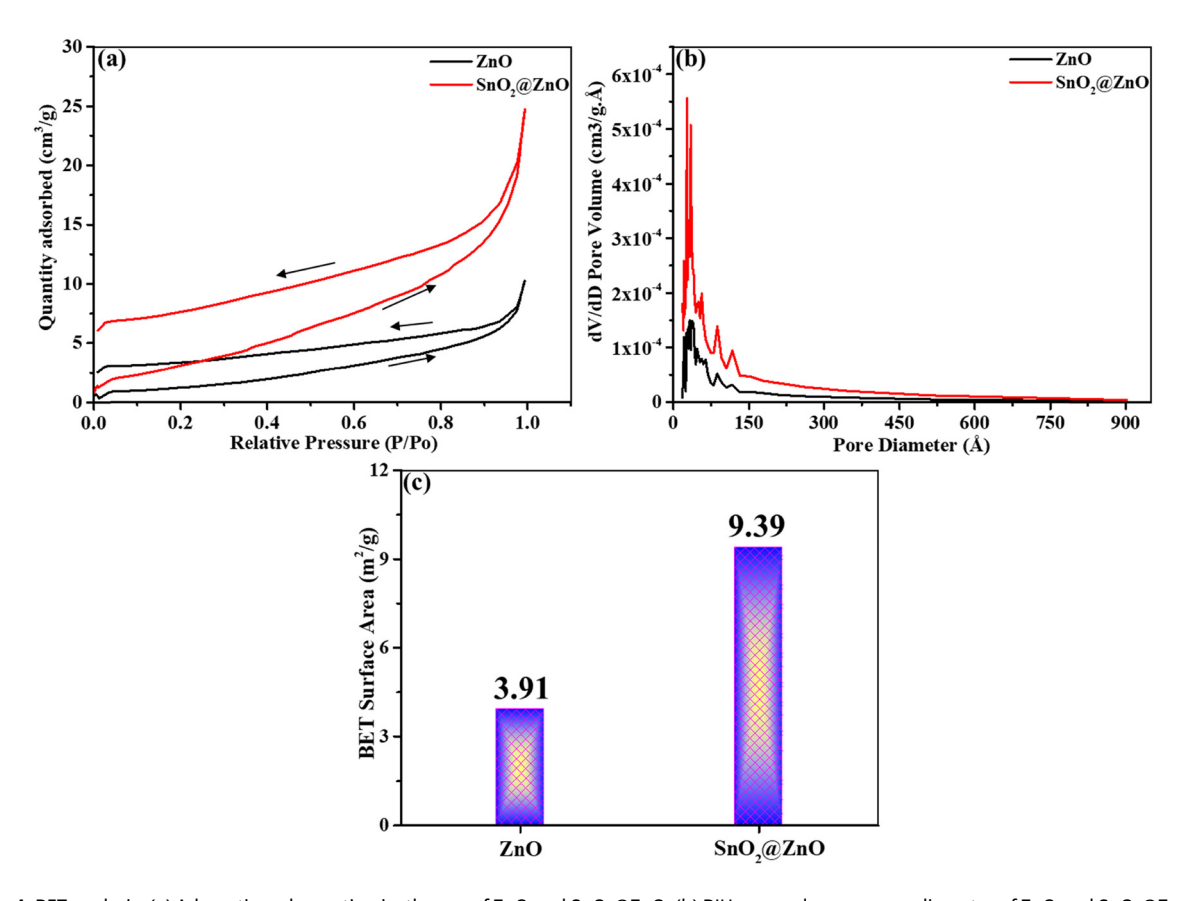


Figure 4: BET analysis. (a) Adsorption–desorption isotherms of ZnO and SnO₂@ZnO, (b) BJH pore volume *vs* pore diameter of ZnO and SnO₂@ZnO, and (c) BET surface area of ZnO and SnO₂@ZnO.

changes are observed in these results. Figure 6(a)–(c) illustrates the deconvolution of the O 1s spectra for ZnO and SnO_2 quantum dots and that of SnO_2 @ZnO reveals a distinct peak at 529.4 eV, attributable to lattice oxygen (O_b). An adsorbed oxygen (O_{ad}) peak also appears at 530.9 eV in the samples, indicating the quality of all materials.

3.2 Three-electrode system electrochemical studies

Electrochemical assessments of the ZnO hexagonal prisms and SnO₂@ZnO nanostructures were conducted within an aqueous electrolyte of 3.0 M KOH. The CV results (Figure 7) show distorted rectangular shapes, suggesting that the electrodes operate in a manner that is characteristic of electric double-layer capacitors (EDLCs). Additionally, the detection of successive redox peaks in the CV profiles of all electrodes suggests the occurrence of faradaic processes during electrochemical cycling. CV signals for ZnO hexagonal prisms (Figure 7(a)) are presented in the voltage

range of 0.1-0.5 V, with varying sweep rates from 5 to 200 mV s^{-1} . The oxidative and reductive peak currents of the ZnO hexagonal prisms exhibit a linear relationship (Figure 7(c)), indicating surface-driven electrochemical behavior stemming from a blend of pseudocapacitance and electric double-layer capacitance [39]. The change in peak positions with increasing scan rates reflects the polarization effects occurring in the system [40].

Figure 7(b) illustrates the CV profiles of $SnO_2@ZnO$ nanostructures at scan rates ranging from 5 to $200\,\text{mV}\,\text{s}^{-1}$ within the voltage range $0.1\text{--}0.5\,\text{V}$. A comparable trend is observed in the electrochemical behavior of both the $SnO_2@ZnO$ samples and the ZnO hexagonal prisms, as they both exhibit a linear association between oxidative and reductive peak currents. The presence of discernible redox peaks implies significant faradaic characteristics inherent in the prepared electrode material [41]. Decoration of SnO_2 quantum dots on ZnO hexagonal prism surfaces enhances the efficiency of electron transfer, boosting both anodic and cathodic currents. From the CV profile of $SnO_2@ZnO$ (Figure 7(d)), the disparity between the reduction and oxidation currents is highlighted, associated with

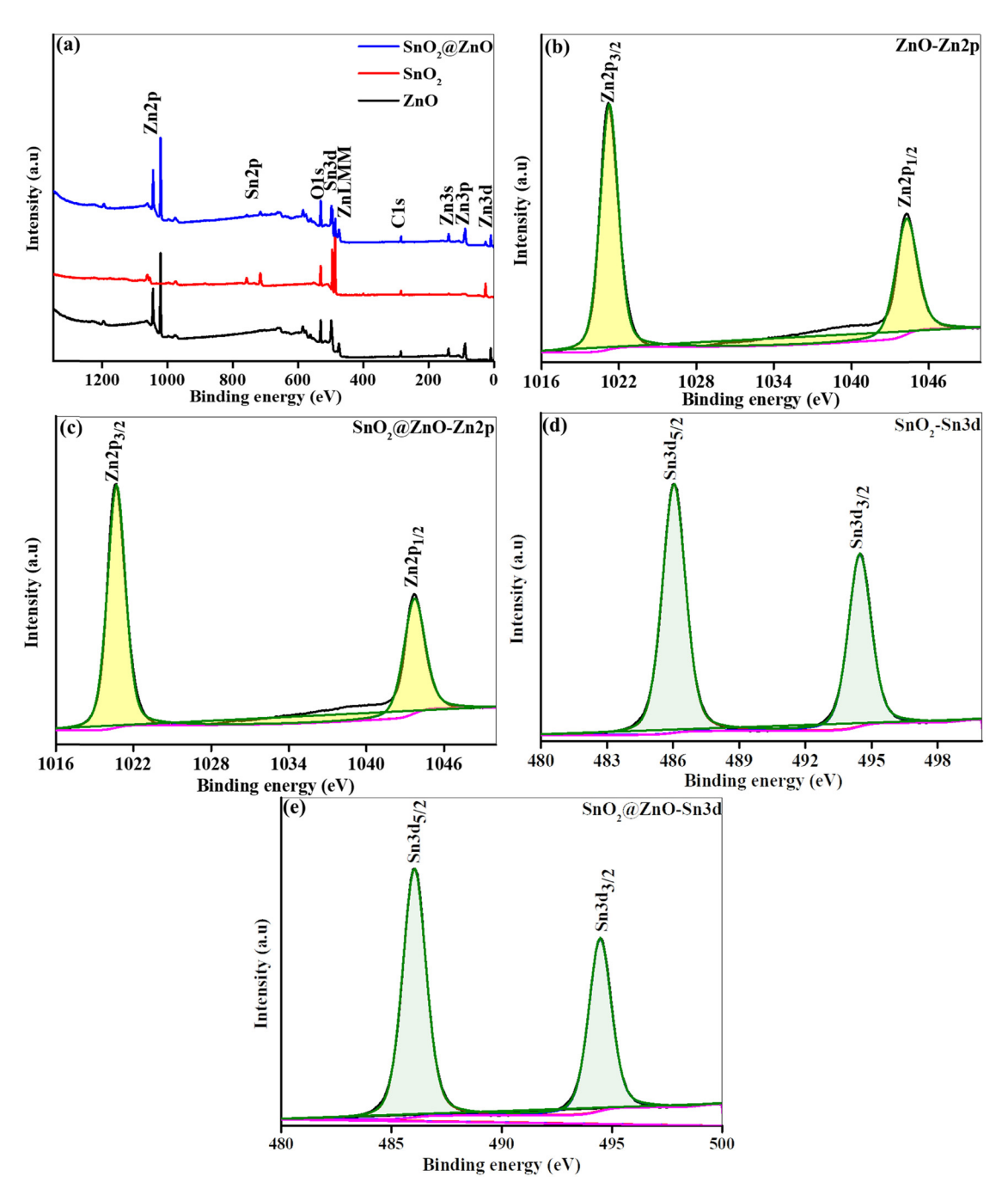


Figure 5: (a) XPS survey spectra of ZnO, SnO₂, and SnO₂@ZnO, (b) and (c) XPS core level spectra of Zn 2p for (b) ZnO and (c) SnO₂@ZnO, and (d) and (e) XPS core level spectra of Sn 3d for (d) SnO₂ and (e) SnO₂@ZnO.

the boosted oxidation peak current. The observed increment in the anodic peak potential ($E_{\rm pa}$) is a result of the synergistic impact of ${\rm SnO_2}$ over ZnO hexagonal prisms, leading to a diminished impedance at the electrode/electrolyte interface. This results in the ZnO electrode displaying a lower anodic peak potential compared to that of the ${\rm SnO_2@ZnO}$ nanostructures. Moreover, while the cathodic peak potential ($E_{\rm pc}$) for ZnO hexagonal prisms

remains lower than that of the $SnO_2@ZnO$ samples, broader peak bases are observed, suggesting a more substantial accumulation of electrons. The association between the scan rate (ν) and the recorded current (I) was explored utilizing the power-law model expressed as equation (4), as postulated by Lindström *et al.* [42].

$$I = p_1 \cdot v^{p_2} = I_{\text{diff}} + I_{\text{cap}}. \tag{4}$$

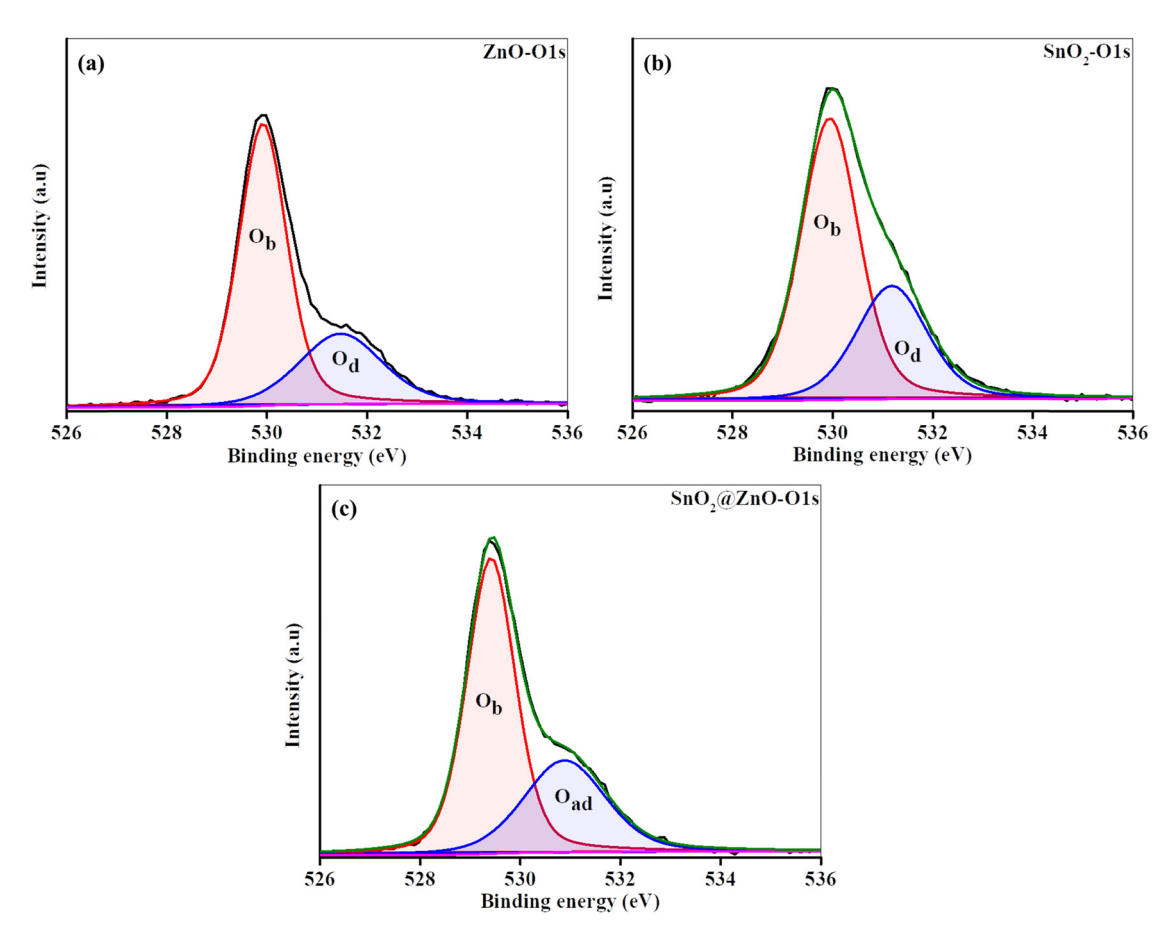


Figure 6: (a)–(c) XPS O 1s spectra for ZnO, SnO₂, and SnO₂@ZnO, respectively.

A linear dependency equation (equation (5)) is employed to fit the experimental data to determine the parameters p_1 and p_2 . This analytical approach facilitates the discernment of diffusion and capacitive-controlled kinetics governing the electrode process, offering key insights into the intrinsic electrochemical performance.

$$\log(I) = \log(p_1) + p_2 \cdot \log(v). \tag{5}$$

The parameter p_2 within the power-law equation offers significant deep insight into the kinetic constraints inherent in the investigated system. A p_2 value near 0.5 suggests that the current is primarily constrained by diffusion. When p_2 = 1, however, it indicates a direct proportionality between the scan rate and current, indicating a surface-controlled (capacitive) process. A p_2 value ranging from 0.5 to 1 implies a combination of diffusion-controlled and capacitive-controlled kinetics. These observations, consistent with prior research [43,44], enhance our comprehension of electrode processes and the complex interaction between diffusion and capacitive-based phenomena. As shown in Figure 7(c), the reductive and oxidative peaks of ZnO hexagonal prisms indicate a p_2 value of about 0.7, signifying the presence of

both diffusion- and capacitive-controlled kinetics. On the contrary, the $SnO_2@ZnO$ electrode depicted in Figure 7(d) exhibits redox peaks with a p_2 of 0.56, indicative of the kinetics influenced by diffusion. In order to precisely quantify the charge accumulation attributed to various mechanisms, the power-law equation can be adjusted to enable a quantitative assessment of the charge contributed by the diffusion-controlled process $(m_2 v^{1/2})$ and the capacitive-type process $(m_1 v)$ as follows [45]:

$$I = m_1 v + m_2 \cdot v^{1/2}, \tag{6}$$

$$\frac{I}{v^{1/2}} = m_1 \cdot v^{1/2} + m_2. \tag{7}$$

In this context, ν denotes the scan rate, I represents the peak current, and m_1 and m_2 are variable parameters. Analysis of the current behavior at different potentials under varying sweep rates yielded the gradient and intercept values of m_1 and m_2 . Across incremental scan rates from 5 to 200 mV s⁻¹, the capacity contributions for the ZnO hexagonal prism electrode (Figure 7(e)) were 14, 19, 25, 32, 36, 40, 42, 44, 47, and 51% of the total current, respectively. These values suggest a combination of both surface-

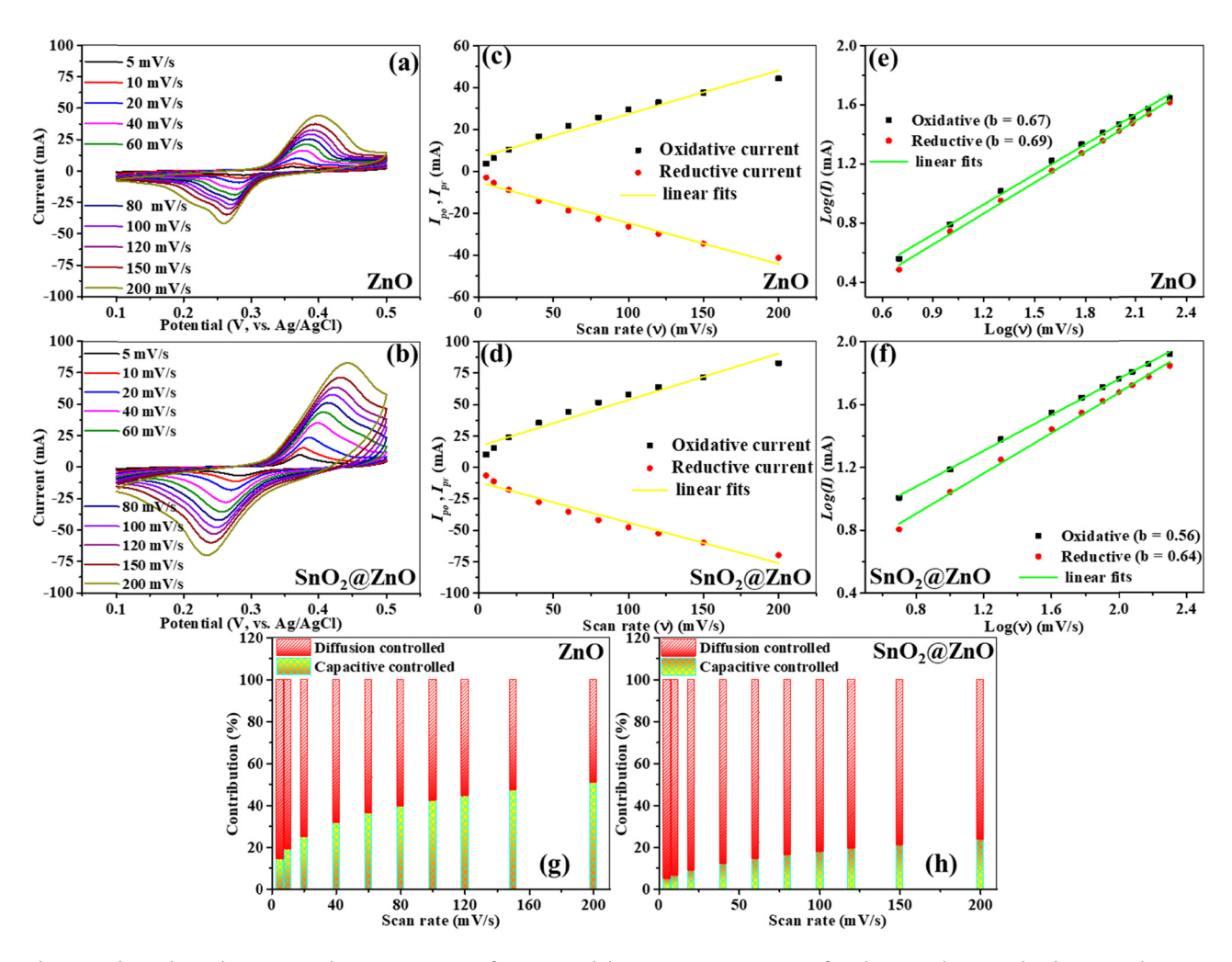


Figure 7: Three-electrode system evaluation. CV curves of (a) ZnO and (b) $SnO_2@ZnO$. Variations of oxidative peak (I_{po}) and reductive peak (I_{pr}) currents *versus* scan rate of (c) ZnO electrode and (d) $SnO_2@ZnO$ electrode. Logarithmic plots of redox peaks for (e) ZnO and (f) $SnO_2@ZnO$. Diffusionand capacitive-controlled contributions of (g) ZnO and (h) $SnO_2@ZnO$.

controlled and diffusion-controlled kinetics. At the same scan rates (Figure 7(f)), the electrode composed of $SnO_2@ZnO$ nanostructures exhibited capacity contributions of 5, 6, 9, 12, 14, 16, 18, 19, 21, and 23% of the total current, respectively, representing a dominant influence of diffusion-controlled kinetics. Figure S1 represents the capacitive and diffusion contribution of ZnO and $SnO_2@ZnO$ samples. This highlights the significant role played by the diffusion-controlled mechanism in determining the charge storage performance of $SnO_2@ZnO$ [46].

The exploration of the charge and discharge behaviors was facilitated by comprehensive GCD measurements, as depicted in Figure 8(a) and (b). Within a spectrum of current densities from 2 to $15~{\rm A~g^{-1}}$, both the ZnO hexagonal prism and SnO₂@ZnO nanostructure electrodes displayed asymmetric behavior in their GCD curves. The non-linear profiles observed for both ZnO hexagonal prisms and SnO₂@ZnO nanostructures indicate the presence of faradaic redox

dynamics that can correspond to the detected oxidation and reduction behavior in the CV profiles. The ZnO hexagonal prisms demonstrated a specific capacitance of 700.68 F g⁻¹, whereas the SnO₂@ZnO electrode exhibited an enhanced specific capacitance of 949.26 F g⁻¹ at a current density of 2 A g⁻¹. As the current density increased to 4, 6, 8, 10, 12, and 15 A g⁻¹, the specific capacitance of the ZnO hexagonal prism electrode reduced to 582, 530, 406, 300, 249, and 219 F g⁻¹, respectively. On the contrary, for the same current densities, the SnO2@ZnO electrode sustained higher specific capacitances of 749, 630, 562, 517, 487, and 459 F g⁻¹ (Figure 8(c)). These findings highlight the superior electrochemical performance of the SnO₂@ZnO electrode, offering higher specific capacitances across different current densities compared to the ZnO hexagonal prism electrode. Both electrodes displayed notable cycling stability, with the ZnO hexagonal prism and SnO2@ZnO electrodes

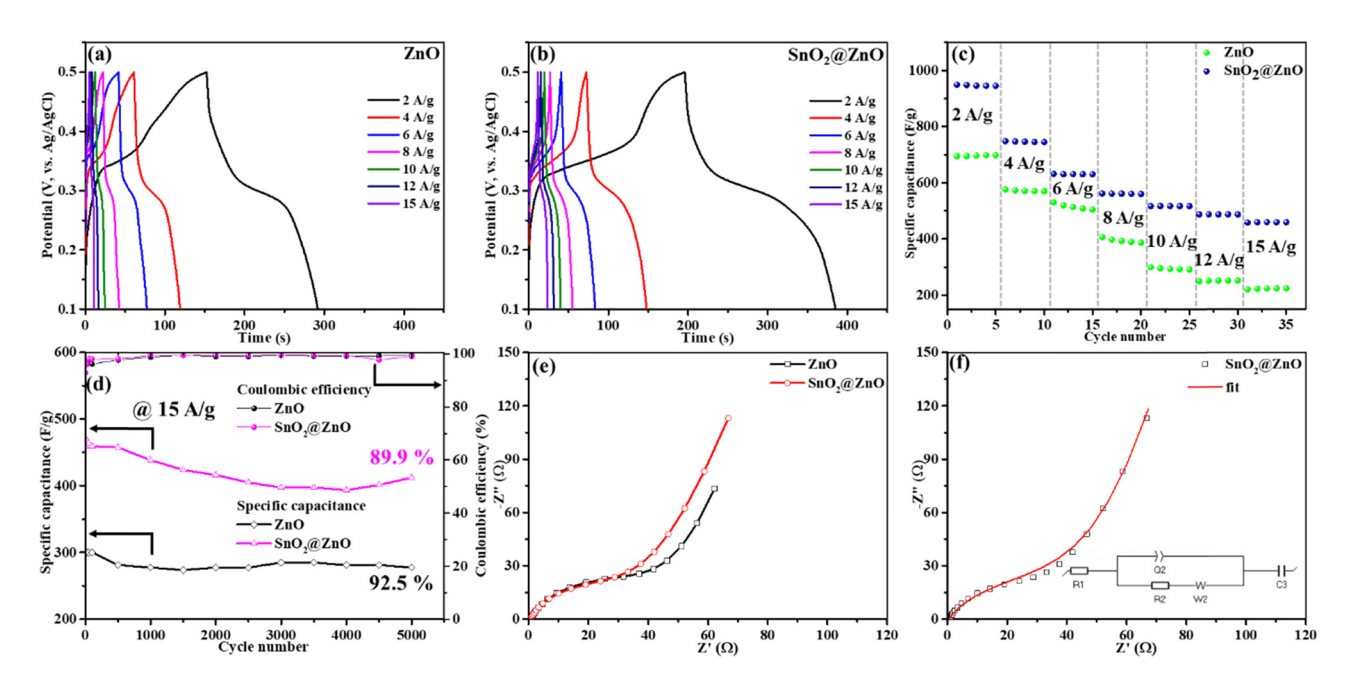


Figure 8: Galvanostatic charge–discharge curves of (a) ZnO and (b) $SnO_2@ZnO$. (c) Specific capacitance vs cycle number at various current densities. (d) Galvanostatic charge–discharge cycling stability of ZnO and $SnO_2@ZnO$ at a current density of 15 A/g for 5,000 cycles. (e) EIS spectra of ZnO and $SnO_2@ZnO$. (f) EIS fitted circuit.

retaining 92.5 and 89.9% of their capacity, respectively, after 5,000 cycles of charge and discharge under an elevated current density of $15\,\mathrm{A\,g^{-1}}$ (Figure 8(d)). Alongside remarkable cycling stability, both the ZnO hexagonal prism and $\mathrm{SnO_2@ZnO}$ electrodes demonstrated consistent Coulombic efficiency.

The EIS technique was utilized to examine the chargetransfer behavior of ZnO hexagonal prism and SnO2@ZnO electrodes, as depicted in Figure 8(e). Figure 8(f) shows the fitted impedance plot along with the corresponding parameters, and the comprehensive values are listed in Table 1. Consistency in the Nyquist plots for all electrodes is achieved by employing an equivalent circuit model. The determined internal impedance (R1) values for the ZnO hexagonal prism and SnO_2 @ZnO electrodes are 0.53 and 0.48 Ω , respectively. The resistance arising from the charge transfer process (R2) for the ZnO hexagonal prism electrode was measured at 50 Ω , higher than that of the SnO₂@ZnO electrode (45 Ω). This implies that the decoration of SnO2 over ZnO hexagonal prisms in the SnO₂@ZnO electrode promotes charge transport between the prisms and quantum dots, thereby enhancing the overall electrochemical performance [47]. The Q2 value, which is a double layer capacitance, for the ZnO hexagonal prism and SnO₂@ZnO electrodes was determined at 3.7 and 2.9 mF s^(α -1), respectively. The pseudocapacitance (C3) values of ZnO hexagonal prisms and SnO₂@ZnO were determined as 0.05 and 0.1F, respectively. The improved electrochemical traits detected for the SnO₂@ZnO electrode, validated by the EIS investigation, corroborate the conclusions

drawn from the GCD and CV assessments, further reinforcing the findings.

3.3 SSC device electrochemical studies

To accurately assess the electrochemical capabilities of the $SnO_2@ZnO$ electrode material, a two-electrode device (SSC) was developed employing SnO_2 -decorated ZnO hexagonal prisms as the positive and negative electrodes. As depicted in Figure 9(a), the CV curves of the fabricated SSC device were recorded at incremental scan rates from 5 to $200\,\mathrm{mV}\,\mathrm{s}^{-1}$, encompassing a potential interval of 0– $1.3\,\mathrm{V}$. Significantly, the CV curves display clearly defined rectangular shapes with evident reduction and oxidation peaks, suggestive of EDLC behavior. The pseudocapacitive behavior of the SSC can be observed owing to the occurrence of a pair of redox peaks. Specifically, even at elevated sweep rates, the CV plots retain their rectangular shapes, highlighting the exceptional rate capability of the SSC. This preservation of rectangular

Table 1: The impedance parameters obtained from fitting for ZnO and $SnO_2@ZnO$ electrodes tested in a three-electrode configuration

Electrode	<i>R</i> 1 (Ω)	R2 (Ω)	Q2 (mF s ^(α-1))	<i>C</i> 3 (F)
ZnO	0.53	50	3.79	0.05
SnO ₂ @ZnO	0.48	45	2.92	0.1

shapes underscores the ability of the SSC to maintain its electrochemical efficiency under heightened scan rates, highlighting its appropriateness for high-rate applications [48]. The CV for the SnO2@ZnO SSC device exhibited a pair of redox peaks (Figure 9(a)), indicating the battery-type behavior of the material [49]. This behavior can also be seen in the GCD results as well. At various current densities (1.2–2 A g⁻¹), the GCD curves of the SnO₂@ZnO SSC were recorded (Figure 9(b)). Across the spectrum of current densities, a noticeable extended discharge time is observed, signifying the advantageous electrochemical behavior of the SSC device and emphasizing its remarkable efficacy in energy storage applications [50]. The SnO₂@ZnO SSC device achieves a consistent specific capacitance of 83 F g⁻¹ (Figure 9(c)) at a current density of 1.2 A g⁻¹. With a rise in the current density to 2 A g⁻¹, a proportional decline in specific capacitance to 19.2 F g⁻¹ is evident. With higher current densities, there is a reduction in specific capacitance due to limitations in charge transfer kinetics and ion diffusion within the electrode material. Such findings underscore the relationship between the applied current density and specific capacitance. To evaluate the enduring capacitance retention of SnO₂@ZnO SSC, a rigorous GCD examination was carried out for an extended period of 5,000 cycles, at 2 A g⁻¹ current density. The results portrayed in Figure 9(d) reveal a consistent capacitance retention of 75% even after enduring 5,000 GCD cycles, showcasing the SSC device's satisfactory cyclic stability. The obtained results emphasize the viability of the SnO₂@ZnO-based SSC for extended energystorage applications. Figure 9(e) illustrates a Ragone plot showcasing the correlation between the power and energy densities of the prepared SSC, computed by means of equations (2) and (3). Remarkably, SnO₂@ZnO SSC displays an energy density of 70.2 W kg⁻¹ at a power density of 2,808 W kg⁻¹, exceeding earlier documented benchmarks for energy and power densities [51-55]. A thorough comparison of these metrics with those of alternative supercapacitor systems is presented in Table 2. The EIS spectrum of the assembled SnO₂@ZnO SSC is depicted in Figure 9(f), which shows a small internal resistance of 0.79 Ω , indicating enhanced specific power capability. An enhanced double-layer capacitance in combination with 62 Ω of minimal charge-transfer resistance emphasizes the decent electrochemical performance of the fabricated SnO2@ZnO device. These results emphasize the promise of the SnO₂@ZnO SSC device for sophisticated energy-storage applications.

Overall, the key findings and advantages observed in the experimental results are as follows:

- XRD analysis confirmed the high crystallinity of ZnO and SnO₂@ZnO, indicating that the introduction of SnO₂ did not alter the hexagonal crystal structure of ZnO but rather enhanced its crystallinity. This structural stability is crucial for maintaining consistent electrochemical performance over multiple cycles.
- FESEM and FETEM imaging revealed well-defined hexagonal prisms with uniform SnO₂ decoration, suggesting effective integration of SnO₂ into ZnO nanostructures.

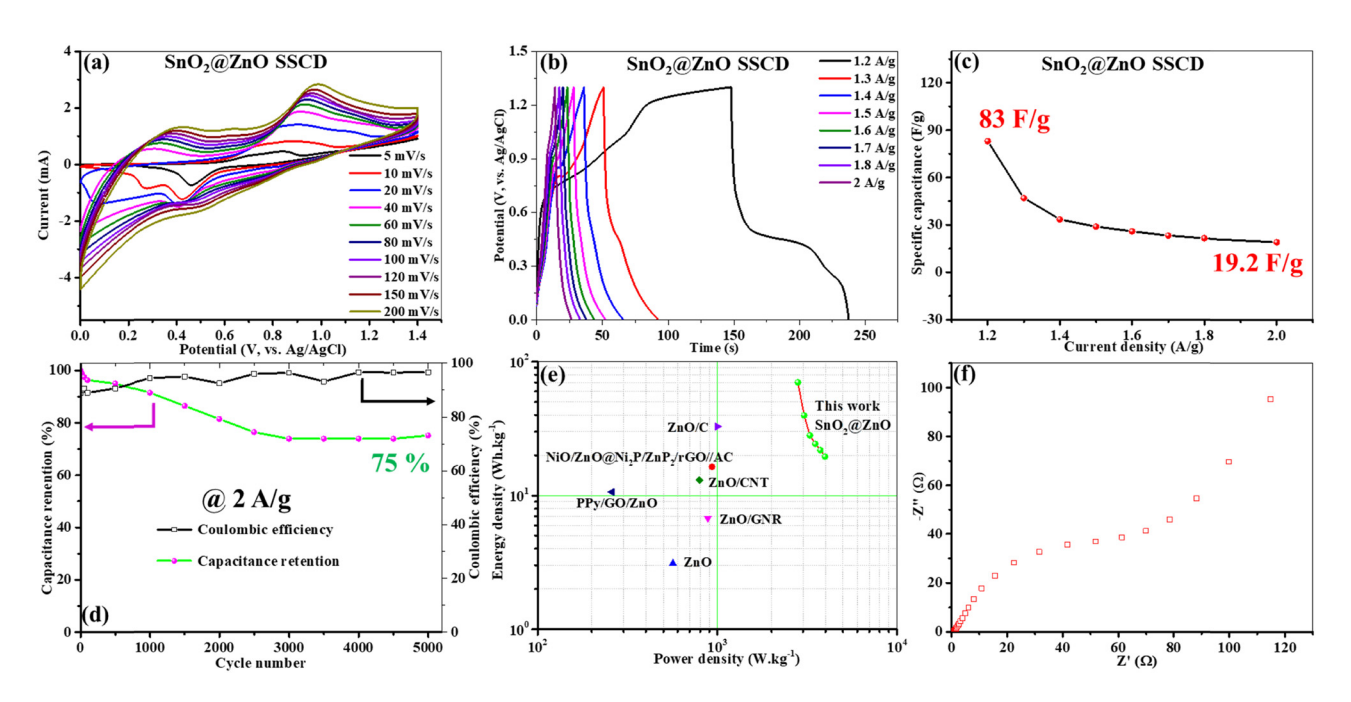


Figure 9: Two-electrode electrochemical evaluation. (a) CV curves, (b) galvanostatic charge–discharge profiles, (c) specific capacitance *vs* current density, (d) capacitance retention and Coulombic efficiency w.r.t. cycle number, (e) Ragone plot, and (f) EIS spectra after 5,000th GCD cycle.

Fable 2: Comparison of the performance of $SnO_2@ZnO$ with various SSCs

Electrodes	Electrolyte	Specific capacitance (F g ⁻¹) Power density (W kg ⁻¹) Energy density (W kg ⁻¹) Capacitance retention	Power density (W kg ⁻¹)	Energy density (W kg ⁻¹)	Capacitance retention	Ref.
NiO/ZnO@Ni2P/ZnP2/rGO//AC HSC	6 М КОН	76 C g ⁻¹	932.74	16.43	91% after 10,000 cycles	[51]
ZnO SSC	0.5 M Na ₂ SO ₄	NA	565	3.1	NA	[52]
ZnO/GNR SSC	0.5 M Na ₂ SO ₄	NA	884	6.8	NA	[52]
ZNO/CNT SSC	0.1 M TBAPC/DMF	48	792	13.1	~95% after 300 cycles	[53]
PPy/GO/ZnO SSC	1 M Na ₂ SO ₄	94.6	258.26	10.65	73.6% after 1,000 cycles	[54]
ZnO/C SSC	1 M Na ₂ SO ₄	92	1,000	32.78	85% after 250 cycles	[55]
SnO ₂ @ZnO SSC	3 M KOH	83.07	2,808	70.2	75% after 5,000 cycles	This work

Additionally, BET analysis demonstrated a threefold increase in the surface area for SnO₂@ZnO compared to that of pristine ZnO, which is advantageous for facilitating more active sites for charge storage and transfer.

- Electrochemical studies, including CV and GCD measurements, showcased superior electrochemical performance of SnO₂@ZnO compared to ZnO alone. SnO₂@ZnO electrodes exhibited higher specific capacitance across various current densities, indicating their ability to store more charge per unit mass and deliver higher energy
- CV profiles of SnO₂@ZnO electrodes displayed well-defined rectangular shapes even at elevated scan rates, indicative of excellent rate capability. Moreover, GCD measurements revealed extended discharge times and consistent capacitance retention over 5,000 cycles, highlighting the enhanced cycling stability of SnO₂@ZnO electrodes.
- Ragone plot analysis demonstrated that the SnO₂@ZnO SSC device achieved higher energy and power densities compared to conventional ZnO-based devices, showcasing their potential for high-performance energy storage applications.

4 Conclusions

In summary, this research introduced a novel electrode material for supercapacitors, comprising SnO2 quantum dots integrated into ZnO hexagonal prisms (SnO2@ZnO), marking the first usage of the SnO₂@ZnO electrode material in supercapacitor application. A comprehensive examination was undertaken to assess the electrochemical performance of the prepared material, yielding significant results. At a current density of 2 A g⁻¹, the ZnO electrode demonstrated a specific capacitance of 700.68 F g⁻¹, while the SnO₂@ZnO electrode demonstrated a specific capacitance of 949.26 F g⁻¹. Notably, both electrodes, SnO₂@ZnO and ZnO, showcased outstanding cycling stability. The SnO₂@ZnO electrode retained a specific capacitance of 412.5 F g⁻¹, whereas the ZnO electrode maintained a specific capacitance of 277.5 F g⁻¹, even after 5,000 cycles at a high current density of 15 A g⁻¹. These results underscore the exceptional robustness and durability of the electrode material. To evaluate the real-world applicability of SnO₂@ZnO, an SSC device was fabricated with SnO₂@ZnO acting as positive and negative electrodes. Remarkably, at a current density of 1.2 A g⁻¹, the SnO₂@ZnO SSC device showcased a decent specific capacitance, achieving 83.07 F g⁻¹. Additionally, remarkable power and energy densities of 2,808 W kg⁻¹ and 70.2 W kg⁻¹, respectively, were achieved. Furthermore, a

significant capacity retention of approximately 75% was exhibited by the SSC device after 5,000 GCD cycles. This underscores the material's ability to endure prolonged cycling while maintaining a consistent electrochemical performance. The outcomes of this investigation provide significant insight into understanding the synthesis and electrochemical attributes of SnO₂@ZnO hexagonal prisms. These findings contribute substantially to the continuous advancement of sophisticated supercapacitors, paving the way for the enhanced optimization and applied integration of SnO₂@ZnO hexagonal prisms in energy-storage systems.

Acknowledgments: This work was supported by Researchers Supporting Project number (RSPD2024R765), King Saud University, Riyadh, Saudi Arabia. This work was supported by the National Research Foundation of Korea (NRF) grant funded by the Korea government (MSIT) (RS-2024-00357072).

Funding information: This work was supported by Researchers Supporting Project number (RSPD2024R765), King Saud University, Riyadh, Saudi Arabia. This work was also supported by the National Research Foundation (NRF) of Korea funded by the Korean government (RS-2023-00280665).

Author contributions: All authors have accepted responsibility for the entire content of this manuscript and approved its submission.

Conflict of interest: The authors state no conflict of interest.

References

- Vaghela P, Pandey V, Sircar A, Yadav K, Bist N, Kumari R. Energy storage techniques, applications, and recent trends: A sustainable solution for power storage. MRS Energy Sustainability. 2023;10:261-76. doi: 10.1557/s43581-023-00069-9.
- Zhang X, Tang Y, Zhang F, Lee C-S, Novel A. Aluminum-graphite dual-ion battery. Adv Energy Mater. 2016;6:1502588. doi: 10.1002/ aenm.201502588.
- Zhang M, Zhang W, Zhang F, Lee C-S, Tang Y. Anion-hosting cathodes for current and late-stage dual-ion batteries. Sci China Chem. 2024;67:1485-509. doi: 10.1007/s11426-023-1957-3.
- Wenkai LI, Ning Z, Zhijie BI, Xiangxin GUO. Na3Zr2Si2PO12 ceramic electrolytes for Na-ion battery: preparation using spray-drying method and its property. J Inorg Mater. 2022;37:189. doi: 10.15541/ jim20210486.
- Wang X, Xia Y, Huang J, Su Y, Chen Z, Chen L, et al. A facile strategy for large-scale production of 2D nanosheets exfoliated by three-roll milling. J Adv Ceram. 2024;13(1):11-8. doi: 10.26599/JAC.2024.9220831.
- Wang X, Luo Z, Huang J, Chen Z, Xiang T, Feng Z, et al. S/N-co-doped graphite nanosheets exfoliated via three-roll milling for high-

- performance sodium/potassium ion batteries. J Mater Sci Technol. 2023;147:47-55. doi: 10.1016/j.jmst.2022.11.015.
- Kumar YA, Alagarasan JK, Ramachandran T, Rezeq M, Bajaber MA, Alalwiat AA, et al. The landscape of energy storage: Insights into carbon electrode materials and future directions. J Energy Storage. 2024;86:111119. doi: 10.1016/j.est.2024.111119.
- Dutta A, Mitra S, Basak M, Banerjee T. A comprehensive review on batteries and supercapacitors: Development and challenges since their inception. Energy Storage. 2023;5:e339. doi: 10.1002/est2.339.
- Ali S, Ahmad T, Tahir MY, Usman M, Chhattal M, Hussain I, et al. The [9] emergence of density functional theory for supercapacitors: Recent progress and advances. J Energy Storage. 2023;73:109100. doi: 10. 1016/j.est.2023.109100.
- [10] Kularatna N, Gunawardane K. Energy storage devices for renewable energy-based systems: rechargeable batteries and supercapacitors. Academic Press; 2021. doi: 10.1016/C2019-0-00796-0.
- Guo W, Yu C, Li S, Qiu J. Toward commercial-level mass-loading electrodes for supercapacitors: opportunities, challenges and perspectives. Energy Env Sci. 2021;14:576-601. doi: 10.1039/D0EE02649B.
- Liu Q, Liu L, Zheng Y, Li M, Ding B, Diao X, et al. On-demand engineerable visible spectrum by fine control of electrochemical reactions. Natl Sci Rev. 2024;11:nwad323. doi: 10.1093/nsr/nwad323.
- Kumar N, Kim S-B, Lee S-Y, Park S-J. Recent advanced supercapacitor: a review of storage mechanisms, electrode materials, modification, and perspectives. Nanomaterials. 2022;12:3708. doi: 10. 3390/nano12203708.
- Pathak M, Bhatt D, Bhatt RC, Bohra BS, Tatrari G, Rana S, et al. High energy density supercapacitors: an overview of efficient electrode materials, electrolytes, design, and fabrication. Chem Rec. 2024;24:e202300236. doi: 10.1002/tcr.202300236.
- [15] Yu H, Zhang J, Shaheen I, Ahmad M, Chen X, Akkinepally B, et al. Natureresembled nanostructures for energy storage/conversion applications. J Ind Eng Chem. 2024;129:53-68. doi: 10.1016/j.jiec.2023.08.041.
- Shah SS, Niaz F, Ehsan MA, Das HT, Younas M, Khan AS, et al. Advanced strategies in electrode engineering and nanomaterial modifications for supercapacitor performance enhancement: A comprehensive review. J Energy Storage. 2024;79:110152. doi: 10. 1016/j.est.2023.110152.
- [17] He J, Cao L, Cui J, Fu G, Jiang R, Xu X, et al. Flexible energy storage devices to power the future. Adv Mater. 2024;36:2306090, doi: 10. 1002/adma.202306090.
- [18] Parveen N. Resent development of binder-free electrodes of transition metal oxides and nanohybrids for high performance supercapacitors - A review. Chem Rec. 2024;24:e202300065. doi: 10. 1002/tcr.202300065.
- Cao X-M, Chen J-Q, Zhao X-R, Ge H, Liu D, Wu Q, et al. Facile synthesis of bead-chain structured MWCNTs@CeO2 with oxygen vacancies-rich for promoting electrochemical energy storage. Chem Eng J. 2024;479:147663. doi: 10.1016/j.cej.2023.147663.
- [20] Akkinepally B, Kumar GD, Reddy IN, Rao HJ, Nagajyothi PC, Alothman AA, et al. Investigation of supercapacitor electrodes based on MIL-101(Fe) metal-organic framework: evaluating electrochemical performance through hydrothermal and microwave-assisted synthesis. Crystals. 2023;13:1547. doi: 10.3390/cryst13111547.
- Aizudin M, Fu W, Pottammel RP, Dai Z, Wang H, Rui X, et al. Recent advancements of graphene-based materials for zinc-based batteries: beyond lithium-ion batteries. Small. 2024;20:2305217. doi: 10.1002/smll.202305217.
- [22] Fei T, Ahmad T, Usman M, Ahmad A, Saleem A, Hanif MB, et al. Zndoped Cr₂O₃ oxides boosted the electrochemical performance of

- aqueous hybrid supercapacitor. Electrochim Acta. 2024;476:143673. doi: 10.1016/j.electacta.2023.143673.
- [23] Wang M, Jiang C, Zhang S, Song X, Tang Y, Cheng H-M. Reversible calcium alloying enables a practical room-temperature rechargeable calcium-ion battery with a high discharge voltage. Nat Chem. 2018;10:667–72. doi: 10.1038/s41557-018-0045-4.
- [24] Mohapatra D, Parida S, Badrayyana S, Singh BK. High performance flexible asymmetric CNO-ZnO//ZnO supercapacitor with an operating voltage of 1.8 V in aqueous medium. Appl Mater Today. 2017;7:212–21. doi: 10.1016/j.apmt.2017.03.006.
- [25] Shi S, Zhuang X, Cheng B, Wang X. Solution blowing of ZnO nanoflake-encapsulated carbon nanofibers as electrodes for supercapacitors. J Mater Chem A. 2013;1:13779–88. doi: 10.1039/C3TA13247A.
- [26] Najib S, Bakan F, Abdullayeva N, Bahariqushchi R, Kasap S, Franzò G, et al. Tailoring morphology to control defect structures in ZnO electrodes for high-performance supercapacitor devices. Nanoscale. 2020;12:16162–72. doi: 10.1039/D0NR03921G.
- [27] Dalapati GK, Sharma H, Guchhait A, Chakrabarty N, Bamola P, Liu Q, et al. Tin oxide for optoelectronic, photovoltaic and energy storage devices: a review. J Mater Chem A. 2021;9:16621–84. doi: 10. 1039/D1TA01291F.
- [28] Yang X, Gong M, Liu Z, Huangfu C, Yan Y, Chi C, et al. Multi-dimensional assembly of ZnO nanodots in the reticular carbon nanofibers for high-performance lithium-ion batteries. Carbon. 2024;223:119001. doi: 10.1016/j.carbon.2024.119001.
- [29] Gaber A, Attia SY, Salem AMS, Mohamed SG, El-Hout SI. Microwaveassisted fabrication of SnO2 nanostructures as electrode for highperformance pseudocapacitors. J Energy Storage. 2023;59:106358. doi: 10.1016/j.est.2022.106358.
- [30] Harisha BS, Akkinepally B, Shim J, Lim J. Hybrid NiO@TiO2 nanoarchitecture for improved electrochemical performance with simulation corroboration. J Energy Storage. 2024;87:111466. doi: 10. 1016/j.est.2024.111466.
- [31] Rafique K, Hassan N, Shah MZU, Al-Saeedi SI, Shah A, Shah MSU, et al. Improved performance in asymmetric supercapacitors using SnO₂–MoS₂ composite microspheres. Surf Interfaces. 2024;44:103650. doi: 10.1016/j.surfin.2023.103650.
- [32] Shaheen Shah S, Oladepo S, Ali Ehsan M, Iali W, Alenaizan A, Nahid Siddiqui M, et al. Recent progress in polyaniline and its composites for supercapacitors. Chem Rec. 2024;24:e202300105. doi: 10.1002/ tcr.202300105.
- [33] Hosseini SM, Safarifard V. MoS2@MOF composites: Design strategies and photocatalytic applications. Mater Sci Semicond Process. 2024;169:107892. doi: 10.1016/j.mssp.2023.107892.
- [34] Sonkar R, Mondal NJ, Boro B, Ghosh MP, Chowdhury D. Cu doped ZnO nanoparticles: Correlations between tuneable optoelectronic, antioxidant and photocatalytic activities. J Phys Chem Solids. 2024;185:111715. doi: 10.1016/j.jpcs.2023.111715.
- [35] Mao W, Wang T, Wang H, Zou S, Liu S. Novel Bi2WO6 loaded g-C3N4 composites with enhanced photocatalytic degradation of dye and pharmaceutical wastewater under visible light irradiation. J Mater Sci: Mater Electron. 2018;29:15174–82. doi: 10.1007/s10854-018-9659-y.
- [36] Shah MSU, Zuo X, Shah A, Al-Saeedi SI, Shah MZU, Alabbad EA, et al. CoSe nanoparticles supported NiSe2 nanoflowers cathode with improved energy storage performance for advanced hybrid supercapacitors. J Energy Storage. 2023;65:107267. doi: 10.1016/j. est.2023.107267.
- [37] Selvaraj Y, Kuzhandaivel H, Nallathambi KS, Elayappan V. Enhanced cyclic stability of cobalt doped Bi25FeO40/BiFeO3 as an electrode

- material for a super long life symmetric supercapacitor device. Energy Fuels. 2023;37:8624–36. doi: 10.1021/acs.energyfuels.3c00135.
- [38] Zhang D. Enhanced photocatalytic activity for titanium dioxide by co-modification with copper and iron. Transit Met Chem. 2010;35:933–8. doi: 10.1007/s11243-010-9414-6.
- [39] Goswami S, Dillip GR, Nandy S, Banerjee AN, Pimentel A, Joo SW, et al. Biowaste-derived carbon black applied to polyaniline-based high-performance supercapacitor microelectrodes: Sustainable materials for renewable energy applications. Electrochim Acta. 2019;316:202–18. doi: 10.1016/j.electacta.2019. 05.133.
- [40] Park HW, Na B-K, Cho BW, Park S-M, Roh KC. Influence of vanadium doping on the electrochemical performance of nickel oxide in supercapacitors. Phys Chem Chem Phys. 2013;15:17626–35. doi: 10. 1039/C3CP52498A.
- [41] Roy N, Mangiri R, Phaneendra Reddy G, Manohar A, Chung E, Deva Prasad Raju B, et al. Carbon nanofiber-supported elongated square bipyramid-like MnWO4 composite electrodes for high-performance battery-type supercapacitors: Enhanced electrochemical performance via synergistic effect. J Electroanal Chem. 2023;947:117764. doi: 10.1016/j.jelechem.2023.117764.
- [42] Lindström H, Södergren S, Solbrand A, Rensmo H, Hjelm J, Hagfeldt A, et al. Li+ ion insertion in TiO₂ (Anatase). 1. Chronoamperometry on CVD films and nanoporous films. J Phys Chem B. 1997;101:7710–6. doi: 10.1021/jp970489r.
- [43] Liu T-C, Pell WG, Conway BE, Roberson SL. Behavior of molybdenum nitrides as materials for electrochemical capacitors: comparison with ruthenium oxide. J Electrochem Soc. 1998;145:1882. doi: 10.1149/1.1838571.
- [44] Aoki K, Tokuda K, Matsuda H. Theory of linear sweep voltammetry with finite diffusion space: Part II. Totally irreversible and quasireversible cases. J Electroanal Chem Interfacial Electrochem. 1984;160:33–45. doi: 10.1016/S0022-0728(84)80113-8.
- [45] Su Y, Shang J, Liu X, Li J, Pan Q, Tang Y. Constructing π–π superposition effect of tetralithium naphthalenetetracarboxylate with electron delocalization for robust dual-ion batteries. Angew Chem Int Ed. 2024;63:e202403775. doi: 10.1002/anie. 202403775.
- [46] Pallavolu MR, Nallapureddy RR, Goli HR, Banerjee AN, Reddy GR, Joo SW. Bioinspired tailoring of nanoarchitectured nickel sulfide@nickel permeated carbon composite as highly durable and redox chemistry enabled battery-type electrode for hybrid supercapacitors. J Mater Chem A. 2021;9:25208–19. doi: 10.1039/ D1TA08122E.
- [47] Palani NS, Kavitha NS, Venkatesh KS, Kumar KA, Senthilkumar M, Pandurangan A, et al. The synergistic effect of the RuO₂ nanoparticle-decorated V2O5 heterostructure for high-performance asymmetric supercapacitors. N J Chem. 2021;45:14598–607. doi: 10.1039/ D1NJ00011J.
- [48] Omar FS, Numan A, Duraisamy N, Bashir S, Ramesh K, Ramesh S. Ultrahigh capacitance of amorphous nickel phosphate for asymmetric supercapacitor applications. RSC Adv. 2016;6:76298–306. doi: 10.1039/C6RA15111F.
- [49] Hussain I, Mak T, Zhang K. Boron-doped trimetallic Cu-Ni-Co oxide nanoneedles for supercapacitor application. ACS Appl Nano Mater. 2021;4:129–41. doi: 10.1021/acsanm.0c02411.
- [50] Ghaly HA, El-Deen AG, Souaya ER, Allam NK. Asymmetric supercapacitors based on 3D graphene-wrapped V2O5 nanospheres and Fe3O4@3D graphene electrodes with high power and energy

- densities. Electrochim Acta. 2019;310:58-69. doi: 10.1016/j. electacta.2019.04.071.
- [51] Mao M, Cui L, Yang K, Xue T, An J, Yao M, et al. Ni2P/ZnP2 nanocrystals/rGO decorated on NiO/ZnO nanoflakes as a high-performance cathode for flexible hybrid supercapacitor. J Energy Storage. 2023;73:109226. doi: 10.1016/j.est.2023.109226.
- [52] Sahu V, Goel S, Sharma RK, Singh G. Zinc oxide nanoring embedded lacey graphene nanoribbons in symmetric/asymmetric electrochemical capacitive energy storage. Nanoscale. 2015;7:20642-51. doi: 10.1039/C5NR06083D.
- [53] Aravinda LS, Nagaraja KK, Nagaraja HS, Bhat KU, Bhat BR. ZnO/ carbon nanotube nanocomposite for high energy density super-

- capacitors. Electrochim Acta. 2013;95:119-24. doi: 10.1016/j. electacta.2013.02.027.
- Chee WK, Lim HN, Harrison I, Chong KF, Zainal Z, Ng CH, et al. [54] Performance of flexible and binderless polypyrrole/ graphene oxide/zinc oxide supercapacitor electrode in a symmetrical two-electrode configuration. Electrochim Acta. 2015;157:88-94. doi: 10.1016/j.electacta.2015. 01.080.
- [55] Sasirekha C, Arumugam S, Muralidharan G. Green synthesis of ZnO/carbon (ZnO/C) as an electrode material for symmetric supercapacitor devices. Appl Surf Sci. 2018;449:521-7. doi: 10.1016/ j.apsusc.2018.01.172.